polymer reports

Sphere sizes in diblock copolymers: discrepancy between electron microscopy and small-angle scattering results

C. V. Berney, R. E. Cohen* and F. S. Bates*

Department of Nuclear Engineering and Department of Chemical Engineering, Massachusetts Institute of Technology, Cambridge, Massachusetts* 02139, *USA*

(*Received* 15 *December* 1981; *revised* 11 *March* 1982)

Five diblock copolymers consisting of polybutadiene spheres in a polystyrene matrix were synthesized and characterized using several techniques, including transmission electron microscopy and small-angle neutron scattering (SANS). The mean radius of the polybutadiene spheres as measured from the electron micrographs was found to be significantly smaller than the SANS value for each of the samples (the average value of R_{EM}/R_{SANS} was 0.77). This discrepancy is greater than can be accounted for by sphere truncation when sectioning the sample for the electron microscope and is believed to be an artifact of the staining procedure.

Keywords polystyrene; polybutadiene; diblock copolymers; electron microscopy; small-angle scattering; sphere sizes

INTRODUCTION

Electron microscopy furnishes direct visual evidence of structures larger than a few Ångstroms, and thus (when carefully calibrated) should be the most reliable technique for determining particle sizes in a wide range of samples. In particular, this technique has been invaluable in the study of the morphologies and particle sizes obtained in microphase-separated block copolymers. When these materials are examined in an electron microscope, however, the sample must often be stained, then microtomed, and finally mounted in a vacuum and bombarded by a beam of electrons. It is conceivable that any one of these steps might perturb the apparent size of the structures examined. In addition, as Roche and Thomas[1] have pointed out, the electron beam itself is subject to manipulation in the instrument, and focusing parameters must be well-defined for an accurate size determination.

For block copolymers of spherical morphology, determination of particle size using the techniques of small-angle X-ray scattering (SAXS) and small-angle neutron scattering (SANS) is relatively straightforward[2-4]. These techniques are applicable to samples of macroscopic dimensions, thus giving information about pristine bulk material unperturbed by sectioning or staining.

In the course of a study of structural and interfacial properties of diblock copolymers, we have synthesized several samples of polystyrene–polybutadiene and subjected them to rigorous characterization by several techniques, including electron microscopy, SAXS and SANS. We find that in all cases, the sphere sizes estimated from the electron micrographs are significantly smaller than those obtained from the small-angle scattering data.

EXPERIMENTAL

This study was carried out on five samples; two of them were polystyrene–polybutadiene diblock copolymers in which normal butadiene was used (SB-1 and SB-7) and two of them were similar diblocks in which perdeuterated butadiene was used to enhance the neutron-scattering properties of the sample (SB_d-1 and SB_d-7). The fifth sample consisted of a diblock (SB_d-3) in which the deuterated polybutadiene chain was comparable in length with the polystyrene segment, which was blended with a quantity of polystyrene homopolymer (S-1) such that the weight fraction of polybutadiene-d_6 was 0.142; we will refer to this blended sample as (S)SB_d-3.

Syntheses were carried out using standard techniques of anionic polymerization[4-6] facilitated by the 'living gels' technique[7]. Molecular weights and distributions were determined for the polystyrene block by analysing samples taken from the reactor prior to butadiene addition, using high-pressure size exclusion chromatography (h.p.s.e.c.). Diblock copolymer compositions were determined by u.v. absorption in chloroform, and each agreed within 1% with that predicted by synthesis stoichiometry. Diblock copolymer molecular weights were then calculated from the combined h.p.s.e.c. and u.v. absorption results; the associated polydispersity index was determined directly by h.p.s.e.c. Characterization results are summarized in *Table 1*.

Table 1 Molecular characterization

Sample	M_{nS}[a]	M_W/M_{nS}[a]	M_{nB}[b]	M_W/M_n[c]	Weight fraction polybutadiene[d]
S-1	64	1.06	–	–	–
SB-1	79	1.06	11	1.06	0.120
SB-7	560	1.08	59	1.11	0.096
SB_d-1	80	1.06	13	1.07	0.136
SB_d-3	78	1.06	54	1.10	0.362[e]
SB_d-7	380	1.07	46	1.10	0.106

[a] Number average molecular weight of the polystyrene fraction (kg mol^{-1}) obtained from h.p.s.e.c. analysis
[b] Number average molecular weight of the polybutadiene fraction (kg mol^{-1}) obtained from M_{nS} and u.v. absorption
[c] Ratio for the entire diblock from h.p.s.e.c.
[d] Obtained from u.v. absorption analysis
[e] Sample contained 10% polystyrene homopolymer before blending

0032-3861/82/081222-05$03.00

Electron microscopy

Transmission electron micrographs for the samples of lower molecular weight (SB_d-1 and SB-1) are shown in *Figure 1*, and micrographs of the three remaining samples are given in *Figure 2*. These were all obtained on a Phillips-200 electron microscope which was operated at 60 kv and calibrated against a diffraction-grating carbon replica (21 600 lines cm^{-1}). Samples were stained with osmium tetroxide[8] and sectioned on an LKB ultramicrotome fitted with a freshly-prepared glass knife. Results from the Phillips instrument were checked by running the samples on a VG HB5 STEM (scanning transmission electron microscope). Agreement was excellent, although the visual quality of the STEM micrographs was inferior to those shown here.

It is evident from the figures that a morphology of polybutadiene spheres (darkened by preferential OsO_4 staining) in a polystyrene matrix is obtained in all five cases. Sphere sizes and their standard deviations (obtained by measuring a characteristic population of about 100 spheres for each sample) are listed in *Table 2*.

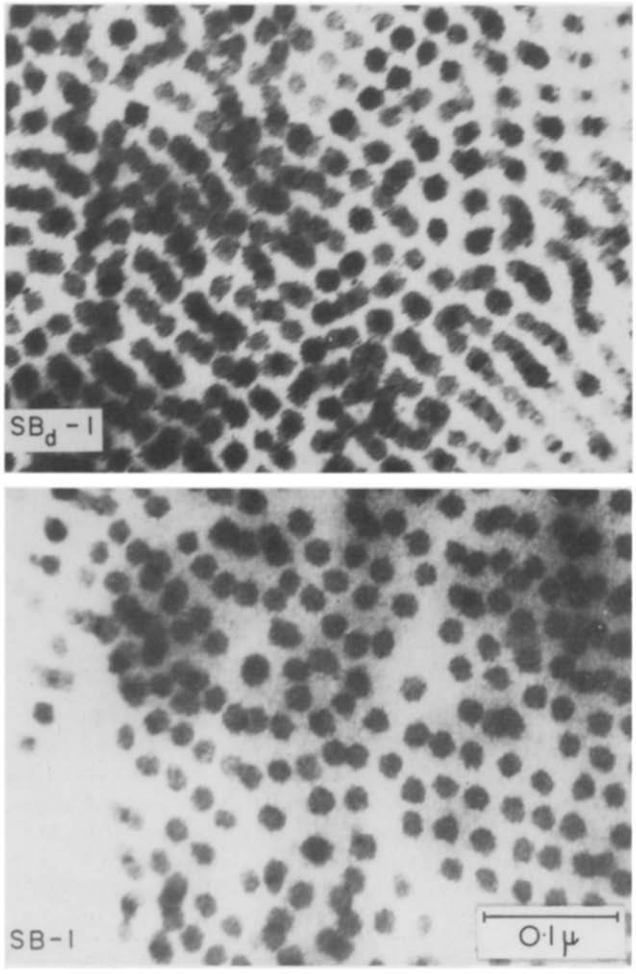

Figure 1 Transmission electron micrographs of SB_d-1 and SB-1. The dark spheres are polybutadiene, which is preferentially stained by the osmium tetroxide. Views shown here were taken near the edge of the slice in order to image the individual spheres more clearly, so they do not illustrate the bcc packing characteristic of the bulk (cf. *Figure 1* of ref. 4)

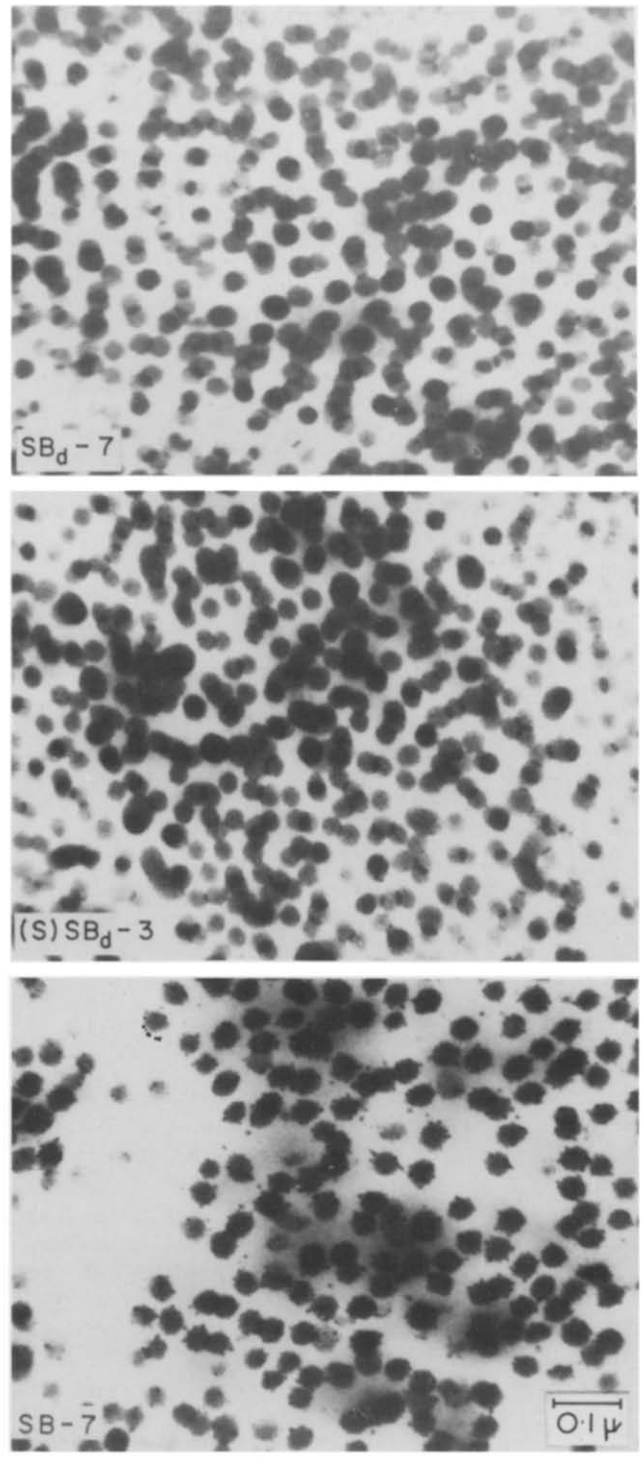

Figure 2 Transmission electron micrographs of SB_d-7, (S)SB_d-3 and SB-7. The dark flecks in the bottom micrograph are probably crystals of osmium tetroxide; they form when the staining process is continued for more than about 3 days

Small-angle scattering

The scattering length[9] of the proton for thermal neutrons is -0.378×10^{-12} cm while that of the deuteron is 0.65×10^{-12} cm. This large difference provides a high contrast between deuterated and undeuterated regions of a material subjected to neutron scattering—in effect, the deuteration provides a 'stain' which permeates the entire volume of the polybutadiene sphere with no significant chemical perturbation.

Table 2 Mean radii of polybutadiene spheres from electron microscopy and SANS

Sample	R_{EM} (Å)[a]	R_{SANS} (Å)[b]	R_{EM}/R_{SANS}
SB-1	90 ± 7	117[c] ± 3	0.77
SB_d-1	94 ± 6	124 ± 2	0.76
SB_d-7	136 ± 9	197 ± 3	0.69
(S)SB_d-3	172 ± 14	221 ± 3	0.78
SB-7	187 ± 17	222 ± 3	0.84

[a] Error represents standard deviation of population sampled
[b] Error represents confidence limits on model fitting
[c] Obtained from Bragg spacing and u.v. analysis assuming bcc packing (see text)

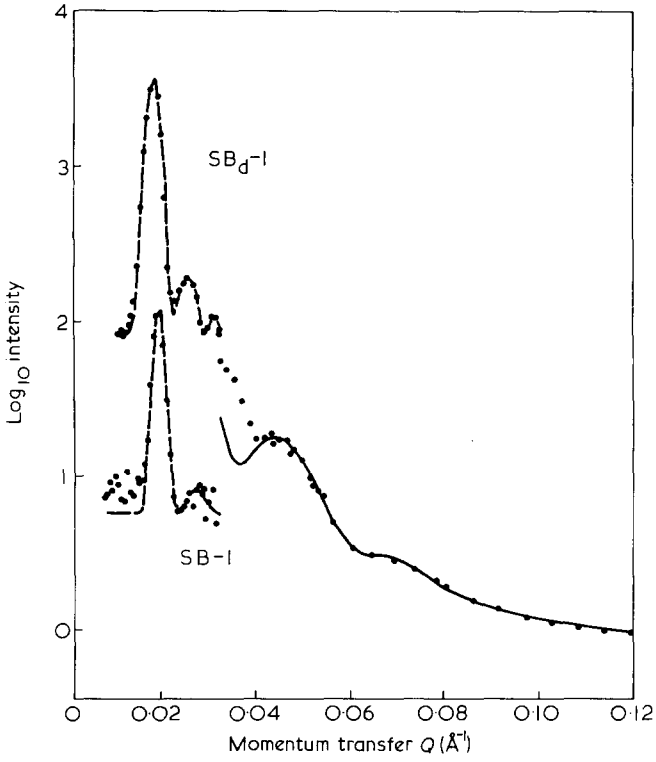

Figure 3 SANS data for SB_d-1 and SB-1. The broken lines represent Gaussian function used to estimate the Q values of the Bragg peaks; they are included here as a guide to the eye. The solid curve represents intraparticle scattering for SB_d-1 as calculated from equation (3) using parameters defined in the text

Small-angle neutron scattering patterns were obtained on the 30-m SANS instrument at the National Center for Small-Angle Scattering Research at Oak Ridge National Laboratory. Neutrons of wavelength $\lambda = 4.75$ Å were used. In order to cover an adequate range of momentum transfer Q (equal to $4\pi\lambda^{-1} \sin\theta$, where θ is half the scattering angle), data were taken at sample-detector distances of 15.3, 7.0, 4.2 and 1.8 m. Composite spectra are shown in *Figures 3* and *4*. The relative intensities for values of Q greater than 0.15 Å^{-1} (not shown in *Figures 3* and *4*) are nearly constant and can be attributed to incoherent scattering. Since incoherent scattering is isotropic, these values have been taken as the incoherent background for all Q.

RESULTS AND DISCUSSION

Scattering from a collection of noninteracting spherical

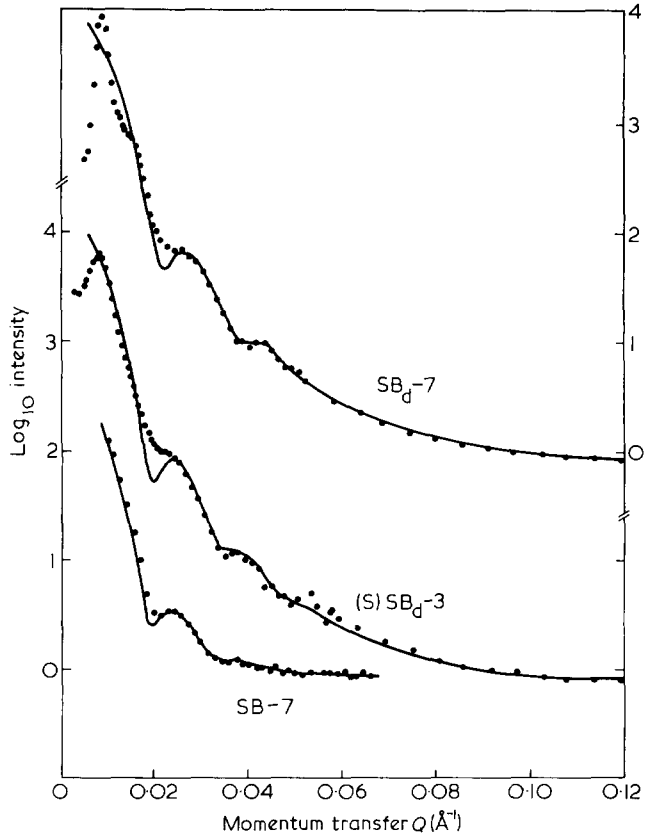

Figure 4 SANS data for SB_d-7, (S)SB_d-3 and SB-7. The solid curves represent intraparticle scattering calculated from equation (1) with parameters adjusted to fit the data. Significant deviations occur below $Q < 0.04$ due to the onset of Bragg effects and multiple scattering

microdomains of radius R can be described[10,11] by the equation

$$I(Q) = K(\rho_B - \rho_S)^2 \int_0^\infty dR\, P(R) f^2(Q,R) \Big/ \int_0^\infty dR\, P(R) \quad (1)$$

where I is the intensity of scattered neutrons, K is a constant depending on neutron flux and detector efficiency, and ρ_B and ρ_S are the particle and matrix scattering-length densities. The quantity f is the single-particle form factor

$$f(Q,R) = \left(\frac{9}{2}\pi\right)^{1/2} \frac{J_{3/2}(QR)}{(QR)^{3/2}} \cdot \exp(-\sigma^2 Q^2/2) \quad (2)$$

In this expression, $J_{3/2}$ is a Bessel function of order 3/2 and the exponential factor models the effect of a diffuse domain boundary in terms of the parameter σ, which can be determined[12] from the Porod region of the scattering curve. We found σ to have essentially the same value (8.5 Å) for all samples studied, a result which will be discussed in more detail in a future report[6]. A Gaussian distribution function $P(R)$ was included to account for dispersion in sphere size[11]:

$$P(R) = \exp[-(R-\bar{R})^2/2\sigma_R^2] \quad (3)$$

The ratio $\sigma_R/\bar{R}$ was between 0.10 and 0.12 for all samples studied.

Figure 3 contrasts the scattering patterns obtained for SB-1 and SB_d-1, samples of similar molecular weight

(*Table 1*) but differing in that deuterated butadiene was used in synthesizing the latter. Using scattering-length densities[13] ρ of 1.416 for polystyrene, 0.415 for polybutadiene, and 6.65 for polybutadiene-d_6 (all in units of 10^{10} cm^{-2}), we find that the ratio of the contrast factor $(\rho_B-\rho_S)^2$ for deuterated and undeuterated samples is around 27, and indeed, this is approximately the ratio of the observed intensities at a given Q value.

The scattering data for samples SB_d-1 (*Figure 3*) can be divided into two regions: Q less than about 0.04 Å^{-1}, where interparticle (Bragg) scattering predominates, and the region at higher Q, where intraparticle scattering (described by equation (1)) is the dominant mechanism.

The positions of the Bragg peaks for SB-1 and SB_d-1 were estimated by fitting Gaussian functions to the data points (broken curves in *Figure 3*); Q values of 0.0193 and 0.0273 Å^{-1} were obtained for SB-1 and 0.0181, 0.0255 and 0.031 Å^{-1} for SB_d-1.

The solid curve extending from $Q\cong 0.03$ to 0.12 Å^{-1} for SB_d-1 represents the calculated intensity for intraparticle scattering obtained from equation (1) with parameters $R=124\pm3$, $\sigma=8\pm1$ and $\sigma_R=15\pm2$ Å (the parameters were determined using an interactive plotting routine; errors quoted represent increments necessary to put the calculated curve into obvious disagreement with the observed data points). The discrepancy between the calculated curve and the observed data below 0.04 Å^{-1} is due to the onset of interparticle scattering, not accounted for in equation (1).

Scattering data for SB-1 were obtained only at $L=15.3$ m, so a similar analysis could not be undertaken. However, since the molecular weights of SB-1 and SB_d-1 differ only slightly and the appearance of the Bragg peaks for the two samples is very similar, it is reasonable to assume that the packing mode for SB-1 is body-centred cubic (bcc), as was established[4] for SB_d-1. Given this assumption, the mean sphere size in SB-1 can be calculated from the size of the unit cell and the volume fraction of polybutadiene. For a bcc lattice, the first Bragg peak is the (110) reflection, and the unit cell length a is $\sqrt{2}[2\pi/Q(110)]=460$ Å. Using densities of 1.05 (S) and 0.895 (B) g cm^{-3} and a weight fraction polybutadiene of 0.120 from the u.v. analysis, we calculate a volume fraction V_B of 0.138. Since bcc packing involves two particles per unit cell, $V_B=2[(4/3)\pi R^3/a^3]$, implying $R=117$ Å. Thus the sphere size in SB-1 is slightly smaller than in SB_d-1, as expected from a comparison of the M_{n_r} values (*Table 1*).

Composite SANS data for SB_d-7, (S)SB_d-3 and SB-7 are shown in *Figure 4*. The solid curves in *Figure 4* again represent model calculations using equation (1); results are shown down to $Q=0.01$ Å^{-1} to demonstrate the discrepancies occasioned by the neglect of interparticle scattering. In these samples a reduced degree of paracrystalline order results in a closer approximation by the model.

Values for the mean radii of the polybutadiene spheres in these five samples are summarized in *Table 2*. In each case the value obtained from electron microscopy is significantly smaller than the SANS result (the average ratio is 0.77). One possible explanation for this discrepancy involves the sectioning carried out in preparing the sample for electron microscopy; the section may contain truncated spheres whose radii (in two-dimensional projection) appear to be smaller than the actual sphere radius. This truncation effect can be estimated quantitatively. For a collection of spheres of radius R in a slice of thickness t, it can readily be shown that

$$\frac{R_{meas}}{R}=\frac{1+\pi R/2t}{1+2R/t} \tag{4}$$

Thus for thick samples, the ratio approaches 1; for $t=R$ (an impossibly thin slice in the present case), the ratio is 0.86, already larger than any of the ratios in *Table 2*. Thicknesses of samples observed microscopically in the present study are estimated to be approximately 500 Å; for this value and $R\cong 200$ Å, the ratio R_{meas}/R goes to 0.90. Thus we conclude that the truncation effect does not account for the bulk of the observed discrepancy.

How reliable are the SANS results? In four of the five cases we have examined, the measured radius depends mainly on the position of the first observed maximum in the intraparticle scattering region. Examination of *Figures 3* and *4* confirms that these maxima are well-defined and easily identified. The positions of these maxima directly yield an initial estimate for R *via* the relationship $QR=5.765$; the modelling we have done with equation (1) refines these estimates and ties them to the bulk of the data in the high Q region by the introduction of the subsidiary variables σ and σ_R/R (which are essentially constant from sample to sample). The R values obtained increase with molecular weight in a consistent manner. Finally, in order to check on whether some unknown interaction with neutrons could lead to a systematic error, a SAXS investigation of SB_d-1 was carried out. While the Bragg region was unresolvable, the data in the intraparticle scattering region were completely consistent with the SANS results. Thus we conclude that the domain radii obtained from the SANS experiments are accurate and reliable.

The corollary to the above conclusion is that there is a systematic error in the sphere sizes obtained from electron microscopy. *Figure 5* shows a log–log plot of sphere radii

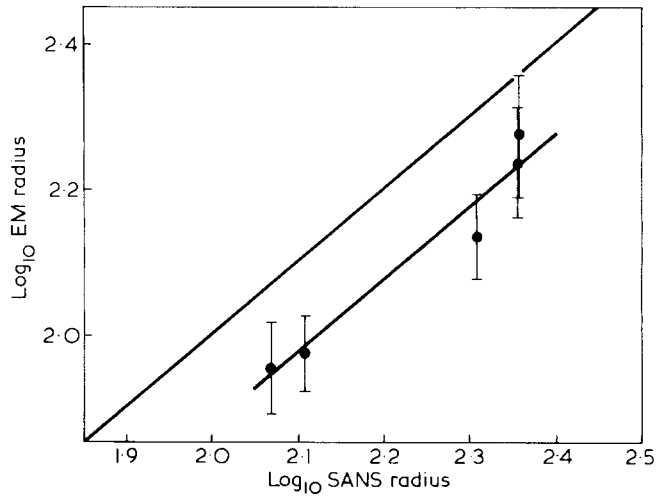

Figure 5 Log–log plot of sphere radii from electron microscopy *versus* SANS results for SB-1, SB_d-1, SB_d-7, (S)SB_d-3, and SB-7 (see *Table 2*). The upper diagonal line represents complete agreement, while the lower line (through the data points) is drawn with a parallel slope and a displacement equal to $\log_{10}$ 0.77 (the mean value of R_{EM}/R_{SANS}). The error bars represent the standard deviation of the EM results, including both the real deviation of sphere size in a given micrograph and the statistical uncertainty due to the finite sample

from electron microscopy *versus* values from neutron scattering. All the EM radii lie below the SANS values, and by about the same amount. Stribeck[15], in a study of lamellar polypropylene utilizing electron microscopy and SAXS, found a similar discrepancy: the lamella thickness he obtained from the EM photos gave values around 30% smaller than those from SAXS analyses. In this case, the samples were stained with chlorosulphonic acid. Inoue *et al.*[16] have noted that the staining procedures they used affected only the outer shell of the microdomains. It seems likely that this is a general characteristic of staining procedures, and one that might be addressed in more detail as a possible source of the discrepancy reported here.

ACKNOWLEDGEMENTS

This research was supported by the National Science Foundation, Division of Materials Research–Polymers Program under grant DMR-8001674 with additional help from DMR-7824185. SANS experiments were performed at the National Center for Small-Angle Scattering Research (NCSASR) which is funded by NSF grant DMR-7724458 through interagency agreement 40637-77 with DOE. The Center is operated by Union Carbide Corporation under DOE contract W-7405-eng-26. The assistance of Dr George Wignall of NCSASR is gratefully acknowledged, and we thank Dr George Hadziioannou of the University of Massachusetts, Amherst, for obtaining the SAXS data. We have also benefitted from the availability of plotting routines developed by Chris Schwier and Martin Suenson, and from stimulating conversations with Dale Handlin and Professor E. L. Thomas of the University of Masschusetts, Amherst.

REFERENCES

1 Roche, E. J. and Thomas, E. L. *Polymer* 1981, **22**, 333
2 Guinier, A. and Fournet, G. 'Small-Angle Scattering of X-Rays', Wiley, New York, 1955
3 Jacrot, B. *Rep. Prog. Phys.* 1976, **39**, 911
4 Bates, F. S., Cohen, R. E. and Berney, C. V. *Macromolecules* 1982, **15**, 589
5 Bates, F. S. *Sc.D. Thesis*, Department of Chemical Engineering, MIT, January 1982
6 Bates, F. S., Berney, C. V. and Cohen, R. E. to be published
7 Bates, F. S. and Cohen, R. E. *Macromolecules* 1981, **14**, 881
8 Kato, K. *Polym. Lett.* 1966, **4**, 35
9 Bacon, G. E. 'Neutron Diffraction', Oxford, London, 1962
10 Hosemann, R. and Bagchi, S. N. 'Direct Analysis of Matter by Diffraction', North Holland, Amsterdam, 1962
11 Hashimoto, T., Fujimura, M. and Kawai, H. *Macromolecules* 1980, **13**, 1660
12 Koberstein, J. T., Morra, B. and Stein, R. S. *J. Appl. Crystallogr.* 1980, **13**, 34
13 Richards, R. W. and Thomason, J. L. *Polymer* 1981, **22**, 581
14 Warren, B. E. *J. Appl. Crystallogr.* 1978, **11**, 695
15 Stribeck, N. *Ph.D. dissertation*, Philipps-Universität, Marburg/Lahn, 1980
16 Inoue, T., Soen, T., Hashimota, T. and Kawai, H. *Macromolecules* 1970, **3**, 87

Monte Carlo simulation of radiation-induced solid state polymerization

Piotr Romiszowski and Andrzej Kolinski
Department of Chemistry, University of Warsaw, 02-093 *Warsaw, Poland*
(*Received* 13 *July* 1981; *revised* 19 *February* 1982)

A Monte Carlo method was used for a computer simulation of radiation-induced solid state polymerization. The propagation of polymer chains was simulated by means of self-avoiding random walks on a tetrahedral lattice. The initiation and termination of the chains were modelled by pseudo-random processes. The influence of conditions of the in-source process on the post-polymerization kinetics and on the degree of polymerization of the polymers was studied.

Keywords Polymerization; Monte Carlo simulation; radiation-induced polymerization; post-effect; kinetics; random walk

INTRODUCTION

This report is a continuation of former papers on the computer simulation of solid state polymerization processes using Monte Carlo methods. The first paper[1] considered a model of post-polymerization neglecting chain growth during the irradiation. In the second[2], a radiation-induced in-source solid state polymerization model was presented. Both these models were idealized descriptions of real, two-stage polymerization processes.

It is the intention of this report to combine the two aforementioned models and examine the results obtained.

When considering the process of solid state polymerization initiated by irradiation, two basic stages can be distinguished:

(1) Formation of new active centres in the irradiated monomer sample and the simultaneous growth of polymeric chains.

(2) Further growth of the chains after removing the sample from the source of radiation (post-polymerization).

In both stages, the termination of chain growth occurs by the trapping of the macroradicals in the mass of the polymer. Such a formulation of the problem is the basis of the pseudostochastic model.

DESCRIPTION OF THE SIMULATIONS

The algorithm constructed is based on the Monte Carlo technique of generating random walks on spatial lattices[3,4]. A tetrahedral lattice was used in the computations. The basic assumptions of the model are the

0032-3861/82/081226-04$03.00